Quantum Chemical Calculations

DFT calculations of various scalar couplings ($^3J_{HN,C'}$, $^3J_{HN,C\beta}$ and $^3J_{HN,H\alpha}$) were carried out on Ace-Xaa-NMe dipeptide analogues (Xaa = Ala or the other amino acid residues listed in Table S1) using Gaussian03[1] running on the Biowulf cluster at the Division of Computer Research and Technology at the National Institutes of Health. In all calculations, ideal local covalent geometries were initially generated with the (ϕ and ψ) backbone angles set to (-60° and -45°) for a "helix" structure and to (-120° and 120°) for a "sheet" structure. After partial geometry optimization using the B3LYP hybrid functional[2] and the 6-311G** basis set, the coupling constants including the Fermi contact (FC), spin-dipolar (SD), paramagnetic spin-orbit (PSO), and diamagnetic spin-orbit (DSO) contributions[3, 4] were then calculated on the resulting geometries at the same level of theory.

Residue type and χ_1 effect on ^3J. The effect of amino acid residue type and sidechain χ_1 rotameric state was investigated by replacing the Ala residue Ace-Ala-NMe. In all cases, the χ_1 torsion angles were set to 60° for the *gauche*+, -60° for the *gauche*-, and 180° for the *trans* configuration in the initial geometry. Values for χ_2 and other side chain torsion angles further removed from the backbone were set to a value found for a particular residue type in the crystal structure of Protein G (PDB code: 1IGD). Except for Asp^- and Glu^-, none of the side chain torsion angles were constrained in the optimization, which resulted in only small deviations (< 20°) from the ideal χ_1 values in the optimized geometry. For Asp^- and Glu^-, due to the interactions between the negatively charged side chain and the amide group, geometry optimization resulted in much larger deviations from the starting, ideally staggered rotamers, and explicit restraints retaining the staggered χ_1 rotamers were used to constrain these angles. To eliminate the effect of variations in bond angles and dihedral angles on couplings to be calculated, all bond angles involving the amide N and the C^α atoms were fixed during the partial geometry optimization, and the ϕ and ψ backbone angles were frozen during the optimization. Improper angles were constrained to maintain peptide planarity during the partial geometry optimization. Calculation of the scalar coupling constants then was performed using the optimized geometry, resulting in the couplings given in Table S1.

Table S1. Calculated ^3J couplings for various residue types.

residue, χ_1 angle	couplings for α-Helix (Hz)			couplings for β-Sheet (Hz)		
	$^3J_{HN-C'}$	$^3J_{HN,C\beta}$	$^3J_{HN,H\alpha}$	$^3J_{HN,C'}$	$^3J_{HN,C\beta}$	$^3J_{HN,H\alpha}$
Ala	1.59	3.93	2.31	0.30	0.77	9.65
Asn, *g*+	1.50	3.57	2.16	0.38	0.39	9.68
Asn, *g*-	1.45	3.64	2.40	0.25	0.69	9.65
Asn, *t*	1.54	3.63	2.41	0.36	0.34	10.25
Asp, *g*+	1.56	2.76	2.82	0.52	0.39	9.76
Asp, *g* -	1.97	2.86	2.56	0.04	1.24	9.51
Asp, *t*	1.73	2.78	2.72	0.28	0.35	10.22
Gln, *g*+	1.69	3.67	2.26	0.28	0.62	9.55
Gln, *g*-	1.57	3.73	2.29	0.34	0.82	9.66
Gln, *t*	1.59	3.80	2.44	0.28	0.72	9.62
Glu, *g*+	1.80	2.92	2.62	0.31	0.63	9.74
Glu, *g*-	1.85	2.81	2.63	0.20	0.91	9.66
Glu, *t*	1.81	3.04	2.66	0.25	0.71	9.71
Ile, *g*+	1.65	3.18	2.31	0.32	0.55	9.59
Ile, *g*-	1.58	3.31	2.41	0.32	0.76	9.64
Ile, *t*	1.66	3.45	2.31	0.33	0.47	9.61
Leu, *g*+	1.61	3.49	2.29	0.33	0.49	9.71
Leu, *g*-	1.57	3.38	2.25	0.30	0.93	9.40
Leu, *t*	1.60	3.69	2.45	0.33	0.63	9.82
Lys, *g*+	1.54	3.87	2.12	0.28	0.57	9.83
Lys, *g*-	1.38	3.92	2.19	0.46	0.57	9.72
Lys, *t*	1.41	4.31	2.24	0.32	0.60	9.63
Phe, *g*+	1.61	3.68	2.25	0.38	0.73	9.59
Phe, *g*-	1.58	3.49	2.43	0.30	0.74	9.82
Phe, *t*	1.58	3.87	2.45	0.34	0.68	9.79
Ser, *g*+	1.47	3.58	2.41	0.29	0.58	9.61
Ser, *g*-	1.64	3.56	2.29	0.23	0.97	9.50
Ser, *t*	1.59	4.25	2.47	0.32	0.64	9.68
Thr, *g*+	1.48	3.32	2.35	0.30	0.62	9.62
Thr, *g*-	1.61	3.42	2.35	0.25	0.89	9.58
Thr, *t*	1.62	3.84	2.40	0.39	0.27	9.86
Trp, *g*+	1.64	3.85	2.29	0.41	0.80	9.59
Trp, *g*-	1.59	3.65	2.44	0.32	0.81	9.82
Trp, *t*	1.58	3.93	2.48	0.35	0.69	9.87
Tyr, *g*+	1.63	3.69	2.27	0.38	0.75	9.58
Tyr, *g*-	1.59	3.51	2.44	0.31	0.76	9.82
Tyr, *t*	1.59	3.88	2.45	0.34	0.69	9.78
Val, *g*+	1.66	3.56	2.33	0.33	0.49	9.61
Val, *g*-	1.65	3.29	2.30	0.32	0.63	9.59
Val, *t*	1.59	3.41	2.39	0.32	0.77	9.65

Effect of H-bonding on ^3J. Effects of H-bonding on the couplings also were studied using the Ace-Ala-NMe dipeptide analogue. Four water molecules were included in the calculation, each of which serves either as a H-bond donor to a carbonyl group or as an acceptor of an amide group. Typical N-H---O=C H-bonding geometries in a helix and a sheet structure were used to construct these backbone-water H-bonds. To study the effect of the amide (or the preceding carbonyl) H-bond on the couplings, the distance between the amide N (or the carbonyl O) atom and the O atom of the water H-bonded to the amide group (or the carbonyl group) was varied from 2.8 to 3.2 Å in a step of 0.1 Å, while the N-O and O-O distances in the other backbone-water H-bonds were kept fixed at 2.8 Å. In addition to the geometric constraints used in the above study of the effect of amino acid residue types, the water oxygen atom positions relative to the backbone are constrained in the partial geometry optimization. Calculation of the scalar coupling constants was then performed using the optimized geometry and the resulting couplings are presented in Table S2. The appreciable effect of the amide H-bond strength on $^3J_{HN,H\alpha}$ is illustrated in Figure S1 for both helical and extended geometry.

Table S2. Calculated ^3J couplings as a function of H-bond length in Ace-Ala-NMe.

residue, H-bond distance	couplings for α-Helix (Hz)			couplings for β-Sheet (Hz)		
	$^3J_{HN-C'}$	$^3J_{HN,C\beta}$	$^3J_{HN,H\alpha}$	$^3J_{HN-C'}$	$^3J_{HN,C\beta}$	$^3J_{HN,H\alpha}$
Ala, N_i-O 2.8 Å	0.93	3.74	3.40	0.18	1.44	8.72
Ala, N_i-O 2.9 Å	0.94	3.75	3.48	0.17	1.44	8.97
Ala, N_i-O 3.0 Å	0.95	3.75	3.54	0.16	1.43	9.16
Ala, N_i-O 3.1 Å	0.95	3.76	3.60	0.15	1.43	9.31
Ala, N_i-O 3.2 Å	0.96	3.75	3.63	0.14	1.42	9.43
Ala, CO_{i-1}-O 2.8 Å	0.93	3.74	3.40	0.18	1.44	8.72
Ala, CO_{i-1}-O 2.9 Å	0.93	3.76	3.39	0.17	1.44	8.72
Ala, CO_{i-1}-O 3.0 Å	0.93	3.77	3.38	0.17	1.44	8.72
Ala, CO_{i-1}-O 3.1 Å	0.93	3.78	3.38	0.16	1.44	8.71
Ala, CO_{i-1}-O 3.2 Å	0.93	3.79	3.37	0.15	1.44	8.71

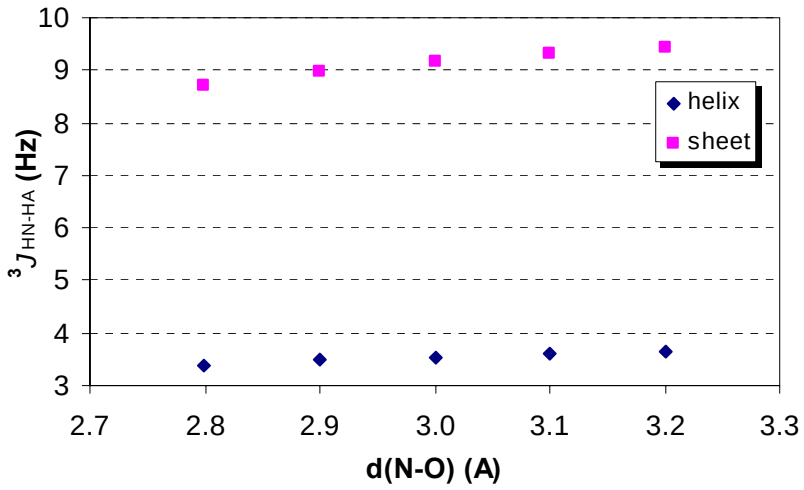

Figure S1. Effect of the amide H-bond length on $^3J_{HN,H\alpha}$ computed for a helical and an extended (sheet) geometry of Ace-Ala-NMe.

Effect of bond angles on ^3J. To investigate how the bond angles of C'_{i-1}-N_i-C^{α}_i, N_i-C^{α}_i-C'_i, and N_i-C^{α}_i-C^{β}_i affect the couplings, a series of calculations were performed using the Ace-Ala-NMe dipeptide analogue in both a helical and extended geometry. In these calculations, one of the above bond angles was independently varied (for C'_{i-1}-N_i-C^{α}_i from 115° to 125°; for N_i-C^{α}_i-C'_i and N_i-C^{α}_i-C^{β}_i from 104.5° to 114.5°). The same geometry constraints as described in the above study of the effect of amino acid residue types were applied during the partial geometry optimization. The optimized geometry was then used for the coupling calculations and the computed couplings are presented in Table S3. Figure S2 shows the dependence of the couplings on the various angles for the helical geometry, whereas for extended structure the analogous graphs are shown in Figure S3.

Table S3. Calculated ^3J couplings as a function of the C'_{i-1}-N_i-C^{α}_i, N_i-C^{α}_i-C'_i, and N_i-C^{α}_i-C^{β}_i angles in Ace-Ala-NMe.

C'_{i-1}-N_i-C^{α}_i angle (deg)	couplings for α-Helix (Hz)			couplings for β-Sheet (Hz)		
	$^3J_{HN,C'}$	$^3J_{HN,C\beta}$	$^3J_{HN,H\alpha}$	$^3J_{HN,C'}$	$^3J_{HN,C\beta}$	$^3J_{HN,H\alpha}$
115	1.30	3.38	2.09	0.14	0.56	9.04
116	1.33	3.50	2.14	0.18	0.60	9.16
117	1.36	3.62	2.19	0.22	0.65	9.27
118	1.40	3.73	2.24	0.26	0.70	9.39
119	1.43	3.85	2.29	0.31	0.74	9.50
120	1.46	3.97	2.34	0.35	0.79	9.61
121	1.49	4.09	2.38	0.39	0.84	9.73
122	1.51	4.20	2.43	0.44	0.89	9.84
123	1.54	4.32	2.47	0.48	0.93	9.95
124	1.57	4.43	2.51	0.53	0.98	10.06
125	1.59	4.54	2.56	0.57	1.03	10.17
N_i-C^{α}_i-C'_i angle (deg)						
104.5	1.32	3.82	2.19	0.49	0.80	9.06
105.5	1.35	3.85	2.22	0.45	0.80	9.17
106.5	1.38	3.88	2.25	0.43	0.80	9.28
107.5	1.41	3.91	2.28	0.40	0.80	9.39
108.5	1.43	3.94	2.31	0.37	0.79	9.50
109.5	1.46	3.97	2.34	0.35	0.79	9.61
110.5	1.48	4.00	2.36	0.33	0.79	9.72
111.5	1.50	4.02	2.38	0.31	0.78	9.83
112.5	1.51	4.05	2.41	0.28	0.78	9.94
113.5	1.53	4.07	2.43	0.27	0.78	10.05
114.5	1.54	4.10	2.44	0.25	0.77	10.15
N_i-C^{α}_i-C^{β}_i angle (deg)						
104.5	1.28	4.19	2.04	0.35	1.00	9.01
105.5	1.32	4.15	2.10	0.35	0.96	9.13
106.5	1.35	4.11	2.16	0.35	0.91	9.25
107.5	1.39	4.06	2.21	0.35	0.87	9.37
108.5	1.42	4.02	2.28	0.35	0.83	9.49
109.5	1.46	3.97	2.34	0.35	0.79	9.61
110.5	1.49	3.92	2.40	0.35	0.75	9.73
111.5	1.53	3.88	2.46	0.35	0.72	9.85
112.5	1.57	3.83	2.53	0.34	0.69	9.97
113.5	1.60	3.78	2.59	0.34	0.66	10.08
114.5	1.64	3.74	2.66	0.33	0.63	10.20

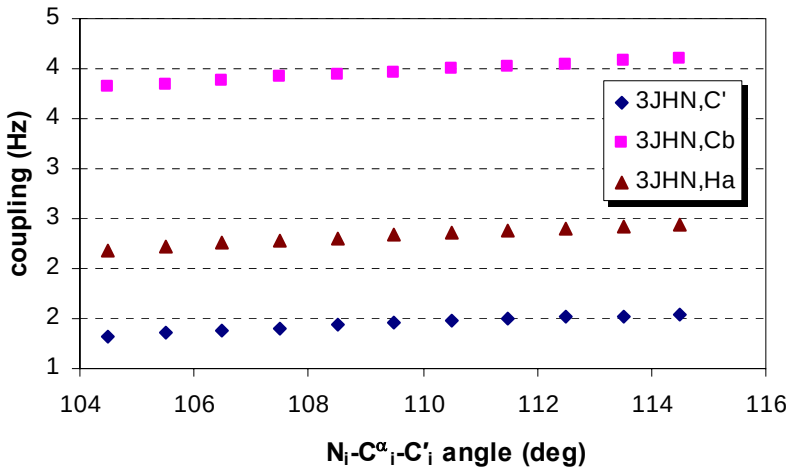

Figure S2. Dependence of various ^{3}J couplings on the N_i-C^{α}_i-C'_i bond angle in a helical geometry of Ace-Ala-NMe.

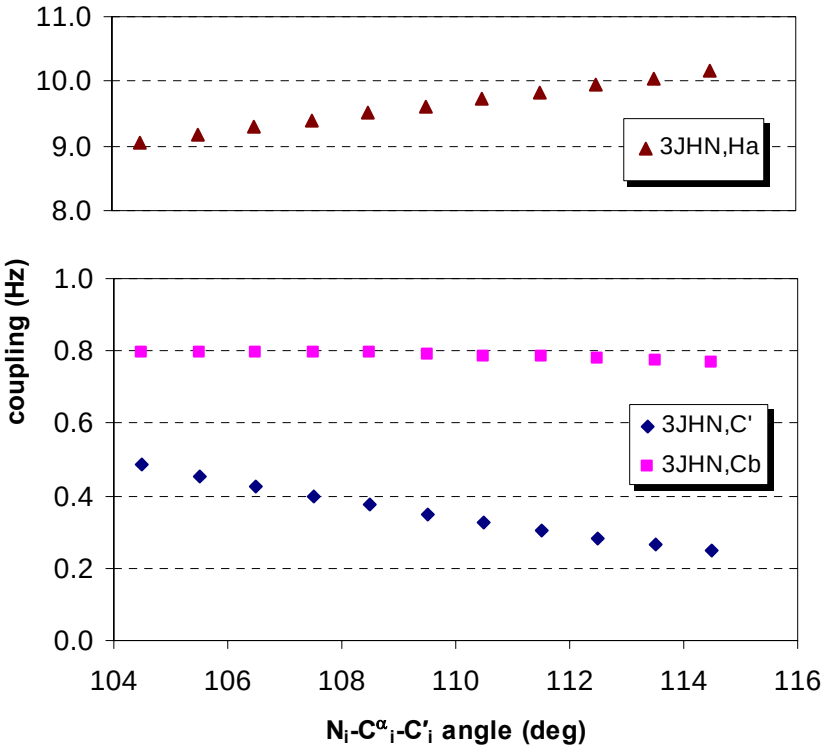

Figure S3. Dependence of various ^{3}J couplings on the N_i-C^{α}_i-C'_i bond angle in an extended geometry of Ace-Ala-NMe.

Table S4. *J* couplings [Hz] and relaxation rates [s^{-1}] from individual experiments.

	ct-MQ($^1H^N$.^{13}Ca)+SQ($^1H^N$)-HNCA				CT-HMQC-J			MQ($^1H^N$.$^{13}C^{\alpha}$)-HNCA		E.COSY	ct-MQ($^1H^N$.$^{13}C^{\alpha}$)-HNCA		E.COSY
	κ=1		κ=2										
	$^3J_{HN,H\alpha}$	$^1J_{C\alpha,H\alpha}$	$^3J_{HN,H\alpha}$	$^1J_{C\alpha,H\alpha}$	$^3J_{HN,H\alpha}$	R_{SQ}	R_{MQ}	$^3J_{HN,C\beta}$	$^1J_{C\alpha,C\beta}$	$^3J_{HN,C\beta}$	$^3J_{HN,C'}$	$^1J_{C\alpha,C'}$	$^3J_{HN,C'}$
Res#													
3	9.58	145.5	9.49	144.6	10.01	4.0	20.3	0.77	32.6	0.66	0.89	51.8	0.62
4	9.88	139.8	9.53	139.6	9.85	4.3	20	1.1	33.9	1.11	0.16	53.1	0.28
5	9.52	142.2	9.56	142.2	9.62	4.7	21.8	0.57	34.7	0.55	0.7	52.0	0.71
6	10.01	140.0	9.6	139.7	9.75	3.4	22.3	1.17	35.3	0.97	0.16	53.3	0.29
7	9.68	140.4	9.52	140.2	9.54	4.6	19.8	1.37	36.2	1.14	0.25	53.4	0.22
8	9.71	140.3	9.66	139.8	10.08	3.5	17.7	0.75	42.5	0.93	0.75	53.7	0.56
9												50.9	
10	4.88	147.2	4.88	147.1	5.11	2.0	22.3	2.87	33.5	2.70	0.91	52.8	0.97
11	10.61	141.6	10.24	141.0	10.2	2.7	18.2	0.91	37.9	0.82	0.32	53.5	0.39
12	7.76	141.6	7.83	141.3	7.89	2.0	18.1	1.5	34.8	1.27	0.78	53.3	0.86
13					9.94	8.5	11.5	0.54	35	0.37	0.88	52.5	1.25
14												51.5	
15	8.44	144.4						0.35	33.5		1.64	52.5	1.69
16	6.8	141.2	6.72	141.0	6.75	2.0	17.6	0.25	38.6	0.12	2.54	51.3	2.69
17					8.98	2.0	17.3	0.18	36.5	0.14	1.49	52.6	1.56
18	6.8	142.8	6.61	142.6	6.77	2.0	18.7	0.18	37.9	0.23	2.49	51.4	2.89
19	9.4	143.2			9.37	2.3	20.5	1.32	35.3	0.99	0.61	52.4	0.45
20	7.22	143.1	7.21	142.9	7.32	2.0	17.6	0.11	33.7	0.09	2.17	52.0	2.24
21	4.11	145.7	4.39	145.9	4.39	2.0	22.2	2.67	33.2	2.60	1.64	53.4	1.98
22	6.3	140.6	6.38	140.8	6.33	2.0	15.9	0.24	35.8	0.19	2.66	52.9	2.92
23	3.0	146.9	3.09	146.6	3.09	2.2	21.6	3.41	33.5	3.08	2.16	53.4	2.03
24	3.87	148.7	3.85	148.8	4.07	2.1	16.4	3.19	33.4	3.01	1.52	52.3	1.54
25	5.35	147						3.35	35.9		0.77	50.7	0.72
26	4.3	148.4	4.3	148.2	4.5	2.0	17.8	3.27	33.5	3.23	1.00	53.0	1.38
27	1.84	148.3	2.03	148.4				3.12	33.4	2.85	2.52	53.0	2.98
28	3.3	148	3.28	148.3	4.08	2.0	19	2.64	33.1	3.00	1.84	52.4	
29	4.66	150	4.71	149.8	4.99	2.0	15.7	3.21	33.2	3.16	0.67	52.1	0.94
30	4.44	144.3	4.57	144.7	5.1	5.2	18.1	2.88	33.2	2.88	0.56	54.7	0.77
31	4.06	146.9	3.99	147.1	4.24	2	19.7	2.93	33.4	2.65	1.13	53.1	1.20
32					5.25	3.8	16.7	3.2	33.7	2.99	0.92	52.6	0.98
33	2.98	152.1	3.1	1526	3.37	2.1	19	3.44	32.0	3.26	1.41	53.2	1.74
34	3.46	146.6	3.67	146.5	3.75	2.4	18.3	3.47	33.3	3.31	1.19	53.6	1.35
35	3.7	150.8						3.2	34.6	3.00	1.3	52.5	1.31
36	3.36	149.7	3.32	149.8	3.98	2.3	16.2	2.41	36.2	2.21	1.9	52.6	2.31
37	9.03	140.3	9.00	138.8	9.56	2.0	15.3	1.71	36.5	1.39	-0.07	53.7	0.11
38												52.8	
39	8.97	142.2	9.03	141.9	8.96	2.0	15.7	1.57	34.8	1.41	0.18	53.6	0.19
40	8.3	142.2	8.29	141.9	8.5	2.3	14.4	0.42	37.8	0.29	1.81	53.1	1.78
41												51.5	
42	8.71	142.1	8.7	141.7	8.76	2.0	18.8	1.68	34.4	1.61	0.04	52.6	0.10
43	8.46	145.8			8.84	2.5	20.2		31.9	1.64	-0.15	52.5	0.06

44	8.94	139.2			8.93	2.0	19	0.16	37.4	0.12	1.81	52.5	1.50
45	8.74	142.1	8.74	141.6	8.85	2.0	19.9	0.34	33.1	0.19	1.21	54.2	1.14
46	9.75	143.1	9.69	142.4	9.96	2.4	18.8	0.79	37.4	0.75	0.64	53.9	0.73
47	3.94	148.1	3.97	147.9	4.15	2.0	20	2.86	33.5	2.76	1.496	52.8	1.38
48			4.21	149.5	4.43	2.0	14.2	2.88	33.3	2.58	1.46	52.9	1.49
49	10.01	138.5	10.13	138.6	10.02	2.5	17.7	1.42	39.3	1.39	-0.01	53.1	0.08
50					7.05	2.0	20.0	1.03	39.4	0.81	2.90	52.0	3.14
51	10.16	142.8	10.1	141.7	10.36	5.7	16.4	0.89	36.7	0.64	0.31	52.8	0.38
52	9.31	145.9			9.58	2.3	23.8	1.69	33.3	1.32	0.01	51.5	0.27
53	9.77	143.9	9.73	143.3	9.63	2.7	20.4	0.30	37.1	0.29	0.97	51.6	1.22
54	10.23	140.8	9.92	140.2	9.84	4.3	20.4	0.21	34.9	0.21	1.11	52.7	1.04
55	9.87	142.6	9.75	142.1	10.00	3.5	22.1	0.98	38.3	0.92	0.23	52.3	0.29
56	8.22	143.7	8.19	1432	8.40	2.0	18.7	2.29	34.5	2.08	0.12	54.0	0.34
Ubiquitin													
46					6.47					0.27			3.58
60					7.26					0.80			2.52
64					7.19					1.35			1.63

Table S5. Backbone ^{3}J couplings in GB3, averaged over multiple measurements and used for all analyses.[a]

Residue	$^{3}J_{HN,H\alpha}$	$^{3}J_{HN,C\beta}$	$^{3}J_{HN,C'}$
Y3	9.8	0.74	0.75
K4	9.8	1.16	0.22
L5	9.6	0.57	0.71
V6	9. 8	1.10	0.22
I7	9.6	1.29	0.23
N8	9.9	0.87	0.66
K10	5.0	2.87	0.94
T11	10.3	0.89	0.35
L12	7.8	1.42	0.82
K13	9.9	0.46	1.06
E15	8.4	0.35	1.67
T16	6.8	0.19	2.61
T17	9.0	0.17	1.52
T18	6.7	0.21	2.69
K19	9.4	1.19	0.53
A20	7.3	0.10	2.20
V21	4.3	2.72	1.81
D22	6.3	0.22	2.79
A23	3.1	3.34	2.10
E24	4.0	3.19	1.53
T25	5.4	3.35	0.74
A26	4.4	3.35	1.19
K28	3.7	2.91	1.84
A29	4.8	3.28	0.81
F30	4.8	2.96	0.67
K31	4.1	2.87	1.17
Q32	5.3	3.18	0.95
Y33	3.2	3.45	1.58
A34	3.7	3.49	1.27
N35	3.7	3.20	1.31
D36	3.7	2.38	2.11
N37	9.3	1.59	0.02
V39	9.0	1.53	0.19
D40	8.4	0.36	1.80
V42	8.7	1.69	0.07

W43	8.7	1.74	-0.05
T44	8.9	0.14	1.66
Y45	8.8	0.27	1.17
D46	9.8	0.79	0.69
D47	4.1	2.89	1.44
A48	4.3	2.81	1.48
T49	10.0	1.45	0.03
K50	7.0	0.95	3.02
T51	10.3	0.78	0.35
F52	9.4	1.55	0.14
T53	9.7	0.30	1.10
V54	10.0	0.22	1.08
T55	9.9	0.98	0.26
E56	8.3	2.25	0.23

[a] $^3J_{HN,H\alpha}$ values represent the average over couplings derived from the CT-MQ($^1H^N$,$^{13}C^\alpha$)+SQ($^1H^N$)-HNCA spectra (averaged over the results from spectra recorded with κ =1 and κ =2), and *J*-modulated HMQC spectra. Based on the pairwise rmsd between these two sets of values, the error in their averaged value equals 0.14 Hz. $^3J_{HN,C\beta}$ values represent the average over couplings derived from the CT-MQ($^1H^N$,$^{13}C^\alpha$)-HNCA spectrum, and a HNCA[CB] E.COSY measurement, where the ^3J values were scaled by 1.06 prior to averaging with the MQ-derived values. Based on the pairwise rmsd between these two sets of values, the random error in their averaged value equals 0.07 Hz. $^3J_{HN,C'}$ values represent the average over couplings derived from a CT-MQ($^1H^N$,$^{13}C^\alpha$)-HNCA spectrum, and a HNCA[C′] E.COSY measurement. Based on the pairwise rmsd between these two sets of values, the random error in their averaged value equals 0.1 Hz.

Table S6. Karplus coefficients and statistical values from fits.

fitting model	# res	pdb code[a]	^3J type	rmsd [Hz]	R[b]	*A*[Hz]	*B*[Hz]	*C*[Hz][c]
rigid	47+3[d]	1P7E	H^N,H^α	0.44	0.983	7.91	-1.28	0.71
			H^N,C'	0.34	0.921	4.05	-1.09	0.10
			H^N,C^β	0.26	0.974	3.46	-0.52	0.16
rigid	47+3	1P7F	H^N,H^α	0.45	0.983	8.00	-1.27	0.62
			H^N,C'	0.32	0.929	4.09	-1.10	0.11
			H^N,C^β	0.28	0.970	3.41	-0.48	0.17
rigid	47+3	1IGD	H^N,H^α	0.68	0.961	7.95	-1.23	0.64
			H^N,C'	0.43	0.869	3.87	-1.15	0.19
			H^N,C^β	0.33	0.958	3.26	-0.38	0.25
rigid	47+3	2OED	H^N,H^α	0.42	0.985	7.97	-1.26	0.63
			H^N,C'	0.31	0.933	4.12	-1.10	0.11
			H^N,C^β	0.25	0.976	3. 51	-0.53	0.14
σ = 10°	35[e]+3	1IGD	H^N,H^α	0.58	0.968	8.28	-1.24	0.53
			H^N,C'	0.39	0.913	4.38	-1.09	-0.04
			H^N,C^β	0.32	0.955	3.53	-0.44	0.14
σ = 0°	35[e]+3	2OED	H^N,H^α	0.31	0.991	8.17	-1.25	0.42
			H^N,C'	0.28	0.956	4.26	-1.06	0.08
			H^N,C^β	0.20	0.983	3.62	-0.58	0.13
σ = 10°	35[e]+3	2OED	H^N,H^α	0.31	0.991	8.69	-1.27	0.16
			H^N,C'	0.28	0.956	4.53	-1.08	-0.05
			H^N,C^β	0.20	0.983	3.85	-0.59	0.02
σ = 20°	35[e]+3	2OED	H^N,H^α	0.31	0.991	10.43	-1.32	-0.71
			H^N,C'	0.28	0.956	5.44	-1.13	-0.51
			H^N,C^β	0.20	0.983	4.63	-0.62	-0.37
motion[f]	47+3	2OED	H^N,H^α	0.49	0.980	8.82	-1.33	0.20
			H^N,C'	0.35	0.918	4.47	-1.09	-0.09
			H^N,C^β	0.28	0.972	3.88	-0.50	-0.07
motion[g]	49[h]+3	1IGD	H^N,H^α	0.63	0.973	8.28[g]	-1.29	0.74
			H^N,C'	0.42	0.886	4.38[g]	-1.05	-0.13
			H^N,C^β	0.38	0.95	3.53[g]	0.04	-0.13
motion[i]	47+3	2OED	H^N,H^α	0.41	0.987	8.17[i]	-1.33	0.51
			H^N,C'	0.32	0.936	4.26[i]	-1.11	0.02
			H^N,C^β	0.24	0.980	3.62[i]	-0.49	0.08
motion[i]	49[h]+3	2OED	H^N,H^α	0.44	0.985	8.17[i]	-1.18	0.63
			H^N,C'	0.34	0.926	4.26[i]	-1.01	0.01
			H^N,C^β	0.26	0.976	3.62[i]	-0.41	0.02

motion[g]	47+3	2OED	H^N,H^α	0.38	0.989	8.69[g]	-1.14	0.39
			H^N,C'	0.31	0.938	4.53[g]	-1.09	-0.09
			H^N,C^β	0.23	0.981	3.85[g]	-0.47	-0.08
motion[g]	49[h]+3	2OED	H^N,H^α	0.38	0.988	8.69[g]	-1.01	0.47
			H^N,C'	0.33	0.931	4.53[g]	-1.06	-0.08
			H^N,C^β	0.23	0.982	3.85[g]	-0.40	-0.12
motion[j]	47+3	2OED	H^N,H^α	0.42	0.986	10.43[j]	-1.27	-0.65
			H^N,C'	0.36	0.921	5.44[j]	-1.05	-0.53
			H^N,C^β	0.26	0.978	4.63[j]	-0.54	-0.32
motion[j]	49[h]+3	2OED	H^N,H^α	0.35	0.990	10.43[j]	-1.12	-0.46
			H^N,C'	0.33	0.927	5.44[j]	-1.18	-0.53
			H^N,C^β	0.23	0.981	4.63[j]	-0.60	-0.37
rigid	47+3	averaged ensemble[k]	H^N,H^α	0.36	0.989	8.19	-1.29	0.46
			H^N,C'	0.31	0.935	4.11	-1.06	0.11
			H^N,C^β	0.21	0.983	3.56	-0.55	0.15
motion[k]	47+3	averaged ensemble[k]	H^N,H^α	0.38	0.988	8.55	-1.31	0.30
			H^N,C'	0.30	0.938	4.37	-1.09	0.00
			H^N,C^β	0.21	0.983	3.69	-0.55	0.07
independent[l]	47+3	ensemble	H^N,H^α	0.36	0.989	8.40	-1.36	0.33
			H^N,C'	0.30	0.937	4.36	-1.08	-0.01
			H^N,C^β	0.22	0.983	3.71	-0.59	0.08

[a] The following RDC restraints were used in NMR structure determination: C^α-C', C'-N and N-H^N (1P7E); C^α-C', C'-N and C^α-H^α (1P7F); C^α-C', C'-N, C^α-H^α and N-H^N (2OED and ensemble).

[b] Pearson's correlation coefficient.

[c] Convention used in equation 4, main text.

[d] "+3" refers to three ubiquitin residues with positive ϕ angles, A46, N60 and E64, included in the fit, using angles from an NMR-refined X-ray structure.[5] Highly dynamic residues 12 and 40 are excluded in the fits.

[e] Residues 10, 20, 21, 23, 24, 25, 32, 34, 36, 39 and 55, which have >1.5 standard deviation in the fits with 47+3 residues, and residue 48, which has $\boldsymbol{S}^2 < 0.75$, were excluded in the fits.

[f] rmsd values of the phi angles from the structure reported in Bouvignies et al.[6] are used for σ. Missing values and those of ubiquitin are set to the gamma amplitude (if available), and otherwise to 10°.

[g] Karplus coefficient "A" is fixed in the fits to the value obtained for the 35+3 "rigid" residues assuming $\sigma = 10°$.

[h] Residues 12 and 40 are included.

[i] Karplus coefficient "A" is fixed in the fits to the value obtained for the 35+3 "rigid" residues assuming $\sigma = 0°$.

[j] Karplus coefficient "A" is fixed in the fits to the value obtained for the 35+3 "rigid" residues assuming $\sigma = 20°$.

[k] Dihedral angles are calculated for each of the 160 ensemble conformers and subsequently averaged. "Rigid" refers to conventional SVD fitting of observed ^3J couplings (all values except for dynamically disordered L12 and D40) to a static structure. "Motion" refers to the results obtained when using eq 5, and rms devations from an averaged ϕ angle is used as σ.

[l] Karplus coefficients are derived from a fit to Karplus equations for each of the 160 ensemble conformers. Since the observed J couplings are linear averages over the coupling of each conformer, the N x M linear equation system (N = number of coupling types, M = number of ϕ angles evaluated) to be minimized is given by:

$$J^{\mathrm{ik,observed}} = \frac{1}{P}\sum_{l=1}^{P} J^{\mathrm{ikl}} = A_{\mathrm{k}}\langle\cos^2(\phi_{\mathrm{il}}+\eta_{\mathrm{ikl}})\rangle + B_{\mathrm{k}}\langle\cos(\phi_{\mathrm{il}}+\eta_{\mathrm{ikl}})\rangle + C_{\mathrm{k}}$$

where $i \in \{1,\ldots,M\}$, $k \in \{1,\ldots,N\}$ and l sums over P ensemble conformers.

Table S7. Root-mean-square ϕ angle related angular fluctuations in GB3 as derived from RDC and ^3J analysis.

		RDC[a]	J Fits 49+3[b]	J Fits 49+3[c]	J Fits 49+3[d]	J Fits 49+3[e]	ensemble
Res#	AA type	σ_γ [degrees]	σ [degrees]	σ [degrees]	σ [degrees]	σ [degrees]	rmsd [degrees]
3	TYR	0	9.8	12.2	20.6	14.5	8.4
4	LYS+	22	10.4	7.5	18.6	15.0	6.6
5	LEU	0	11.2	16.1	22.2	15.8	4.8
6	VAL	21	4.1	7.1	21.2	14.1	6.9
7	ILE	0	9.8	12.1	21.0	14.2	9.0
8	ASN	7	4.5	13.2	21.5	18.6	6.8
9	GLY	2					12.0
10	LYS+	30	13.7	21.3	27.4	23.0	12.2
11	THR	15	2.0	3.7	16.4	13.1	11.8
12	LEU	33	24.2	29.4	35.6	30.0	17.8
13	LYS+	23	7.0	10.5	18.8	13.9	14.6
14	GLY	26					15.7
15	GLU	17	16.7	18.8	24.8	23.2	10.4
16	THR	22	16.9	14.3	23.9	31.2	10.4
17	THR	18	7.7	13.1	20.3	14.2	9.9
18	THR	12	10.3	21.1	18.8	13.0	8.7
19	LYS+	17	13.2	12.8	25.9	20.5	10.1
20	ALA	7	14.1	11.0	18.3	19.9	9.9
21	VAL	0	7.1	19.5	30.1	53.7	10.3
22	ASP	16	6.1	16.5	14.3	32.3	8.4
23	ALA	11	3.6	15.1	17.8	23.9	4.4
24	GLU	19	16.3	3.2	12.4	15.6	14.1
25	THR		6.0	0.7	17.1	9.7	6.2
26	ALA	11	5.7	15.3	18.2	13.2	2.9
28	LYS+	9	13.1	16.8	21.1	24.7	2.1
29	ALA	9	9.5	7.5	13.0	11.5	2.1
30	PHE	11	8.7	12.5	21.2	11.0	2.0
31	LYS+	11	14.1	16.5	21.7	31.3	2.5
32	GLN	10	14.5	9.9	28.4	14.6	3.2
33	TYR	11	6.7	1.2	10.2	4.5	2.1
34	ALA	18	13.8	5.4	15.2	9.8	3.8
35	ASN	10	7.7	7.8	22.1	14.6	7.3
36	ASP	11	13.2	23.2	33.4	26.4	4.7
37	ASN	17	10.7	13.7	21.7	11.6	9.6
38	GLY	17					11.9
39	VAL	17	12.8	1.1	15.9	13.8	12.6
40	ASP	0	16.7	21.2	30.7	31.6	15.8
41	GLY	32					15.4
42	VAL	10	14.7	11.8	24.3	21.3	9.1
43	TRP	1	11.3	19.4	23.6	26.3	6.3
44	THR	5	3.3	18.0	23.4	23.3	6.0
45	TYR	17	20.2	17.0	26.0	13.0	11.1
46	ASP	8	8.7	12.3	20.4	15.1	10.1

47	ASP	4	10.1	16.9	33.7	25.4	9.4
48	ALA	25	14.5	23.7	22.3	37.7	11.6
49	THR	10	0.5	2.0	16.0	13.3	8.8
50	LYS+	17	14.7	21.3	29.0	24.1	3.9
51	THR	0	1.4	1.9	18.0	10.0	8.1
52	PHE	0	6.8	12.6	20.6	15.8	5.6
53	THR	24	6.9	11.6	20.7	10.9	8.2
54	VAL	0	6.6	7.8	18.2	12.9	4.2
55	THR	21	10.7	11.0	18.9	14.0	10.9
56	GLU	18	4.3	14.6	24.4	28.1	16.8
average		13.4	10.1	12.9	21.6	19.2	8.6
standard dev.		9.3	5.0	6.5	5.5	8.9	4.1
Ubiquitin							
46	ALA		10.6	17.5	24.1	22.5	
60	ASN		7.6	21.0	23.9	17.5	
64	GLU		17.9	21.6	23.9	22.3	

[a] From Bouvignies et al.[6]

[b] From fits of the ^{3}J couplings to 2OED, using eq 5, and keeping coefficients *A* fixed at the values reported in Table S6, for the set of "35+3" residues assuming σ = 0°.

[c] From fits of the ^{3}J couplings to 2OED, using eq 5, and keeping coefficients *A* fixed at the values reported in Table S6, for the set of "35+3" residues assuming σ = 10°.

[d] From fits of the ^{3}J couplings to 2OED, using eq 5, and keeping coefficients *A* fixed at the values reported in Table S6, for the set of "35+3" residues assuming σ = 20°.

[e] From fits of the ^{3}J couplings to 1IGD, using eq 5, and keeping coefficients *A* fixed at the values reported in Table S6, for the set of "35+3" residues assuming σ = 10°.

Table S8. $^{3}J_{HN,H\alpha}$ Karplus coefficients from different parameterizations.

fitting model[b]	*A* [Hz]	*B* [Hz]	*C* [Hz]	reference
rigid	8.0	-0.9	0.9	Bystrov, V.F., Portnova, S.L., Tsetlin, V.L., Ivanov, V.T. and Ovchinnikov, Y.A., 1969, Tetrahedron, 25, 493
rigid	7.9	-1.55	1.35	Ramachandran, G.N., Chandrasekaran, R. and Kopple, K.D., 1971, Biopolymers, 10, 2113
rigid	9.4	-1.1	0.4	Bystrov, V.F., Ivanov, V.T., Portnova, S.L., Balashova, T.A. and Ouchinnikov, Y.A., 1973, Tetrahedron, 29, 873
rigid	5.4	-1.3	2.2	DeMarco, A., Llinas, M. and Wuthrich, K., 1978, Biopolymers, 17, 637
rigid	6.4	-1.4	1.9	Pardi, A., Billeter, M. and Wuthrich, K., 1984, J. Mol. Biol., 180,, 741-751
rigid	6.7	-1.3	1.5	Ludvigsen, S., Andersen, K.V., Poulsen, F.M., 1991, J. Mol. Biol., 217, 731-736
rigid	6.0	-1.4	2.4	Smith, L.J., Sutcliffe, M.J., Redfield, C. and Dobson, C.M., 1991, Biochemistry, 30, 986
rigid	6.51	-1.76	1.60	Vuister,G.W. and Bax, A.,1993, J. Am. Chem. Soc., 115, 7772-7777
rigid	6.98	-1.38	1.72	Wang, A.C. and Bax. A., 1996, J. Am. Chem. Soc., 118, 2483-2494
rigid	7.90	-1.05	0.65	Schmidt, J.M., Blumel, M., Lohr, F. and Ruterjans, H., 1999, J. Biomol. NMR, 14, 1-12
rigid	7.13	|B|=0.87	0.10	Habeck, M., Rieping, W. and Nilges, M., 2005, J. Magn. Reson., 177, 160-165
rigid	7.97	-1.26	0.63	Current work, using 2OED as a reference
DFT(Ace-Ala-NMe)	9.44	-1.53	-0.07	Case, D.A., Scheurer, C. and Bruschweiler, J. Am. 2000, Chem. Soc., 116, 11199-11200 R.,
DFT(Ala-Ala-NH_2)	9.14	-2.28	-0.29	Case, D.A., Scheurer, C. and Bruschweiler, J. Am. 2000, Chem. Soc., 116, 11199-11200 R.,
motion	9.5	-1.4	0.3	Bruschweiler, R. and Case, D.A.,1994, J. Am. Chem. Soc., 116, 11199-11200
motion	8.69	-1.14	0.39	Current work, using 2OED as a reference, and assuming $\langle\sigma\rangle=10°$ for "35+3" well-defined residues
ensemble	8.40	-1.36	0.33	Current work, using the 160 member ensemble of Clore, G. M.and Schwieters, C. D., 2006 J. Mol. Biol., 355, 879-886

Table S9. $^{3}J_{HN,C'}$ Karplus coefficients from different parameterizations.

fitting model[b]	*A* [Hz]	*B* [Hz]	*C* [Hz]	reference
rigid	5.7	-2.7	0.1	Seip, S., Balbach, J. and Kessler, H., 1994, J. Magn. Reson. B, 104, 172-179
rigid	5.8	-2.7	0.1	Weisemann, R.,Ruterjans, H., Schwalbe, H., Schleucher, J., Bermel, W. And Griesinger, C., 1994, J. Biomol. NMR, 4, 231-240, origin unclear
rigid	4.0	-1.1	0.1	Wang, A.C. and Bax, A., 1995, J. Am. Chem. Soc., 117, 1810-1813
rigid	4.32	-0.84	0.00	Wang, A.C. and Bax. A., 1996, J. Am. Chem. Soc., 118, 2483-2494
rigid	4.41	-1.36	0.24	Schmidt, J.M., Blumel, M., Lohr, F. and Ruterjans, H., 1999, J. Biomol. NMR, 14, 1-12
rigid	4.19	|B|=0.99	0.03	Habeck, M., Rieping, W. and Nilges, M., 2005, J. Magn. Reson., 177, 160-165
rigid	4.12	-1.10	0.11	Current work, using 2OED as a reference
DFT(Ace-Ala-NMe)	5.58	-1.06	-0.30	Case, D.A., Scheurer, C. and Bruschweiler, J. Am. 2000, Chem. Soc., 116, 11199-11200 R.
DFT(Ala-Ala-NH_2)	5.34	-1.46	-0.29	Case, D.A., Scheurer, C. and Bruschweiler, J. Am. 2000, Chem. Soc., 116, 11199-11200 R.,
motion	4.53	-1.09	-0.09	Current work, using 2OED as a reference, and assuming $\langle\sigma\rangle$=10° for “35+3” well-defined residues
ensemble	4.36	-1.08	-0.01	Current work, using the 160 member ensemble of Clore, G. M.and Schwieters, C. D., 2006 J. Mol. Biol., 355, 879-886

Table S10. $^{3}J_{HN,C\beta}$ Karplus coefficients from different parameterizations.

fitting model[b]	*A* [Hz]	*B* [Hz]	*C* [Hz]	reference
rigid	4.5	-1.5	-0.2	Seip, S., Balbach, J. and Kessler, H., 1994, J. Magn. Reson. B, 104, 172-179
rigid	3.39	-0.94	0.07	Wang, A.C. and Bax. A., 1996, J. Am. Chem. Soc., 118, 2483-2494
rigid	2.90	-0.56	0.18	Schmidt, J.M., Blumel, M., Lohr, F. and Ruterjans, H., 1999, J. Biomol. NMR, 14, 1-12
rigid	3.26	|B|=0.87	0.10	Habeck, M., Rieping, W. and Nilges, M., 2005, J. Magn. Reson., 177, 160-165
rigid	3. 51	-0.53	0.14	Current work, using 2OED as a reference
DFT(Ace-Ala-NMe)	5.15	0.01	-0.32	Case, D.A., Scheurer, C. and Bruschweiler, J. Am. 2000, Chem. Soc., 116, 11199-11200 R.
DFT(Ala-Ala-NH_2)	4.58	-0.36	-0.31	Case, D.A., Scheurer, C. and Bruschweiler, J. Am. 2000, Chem. Soc., 116, 11199-11200 R.,
motion	3.85	-0.47	-0.08	Current work, using 2OED as a reference, and assuming $\langle\sigma\rangle$=10° for “35+3” well-defined residues
ensemble	3.71	-0.59	0.08	Current work, using the ensemble of Clore, G. M.and Schwieters, C. D., 2006 J. Mol. Biol., 355, 879-886

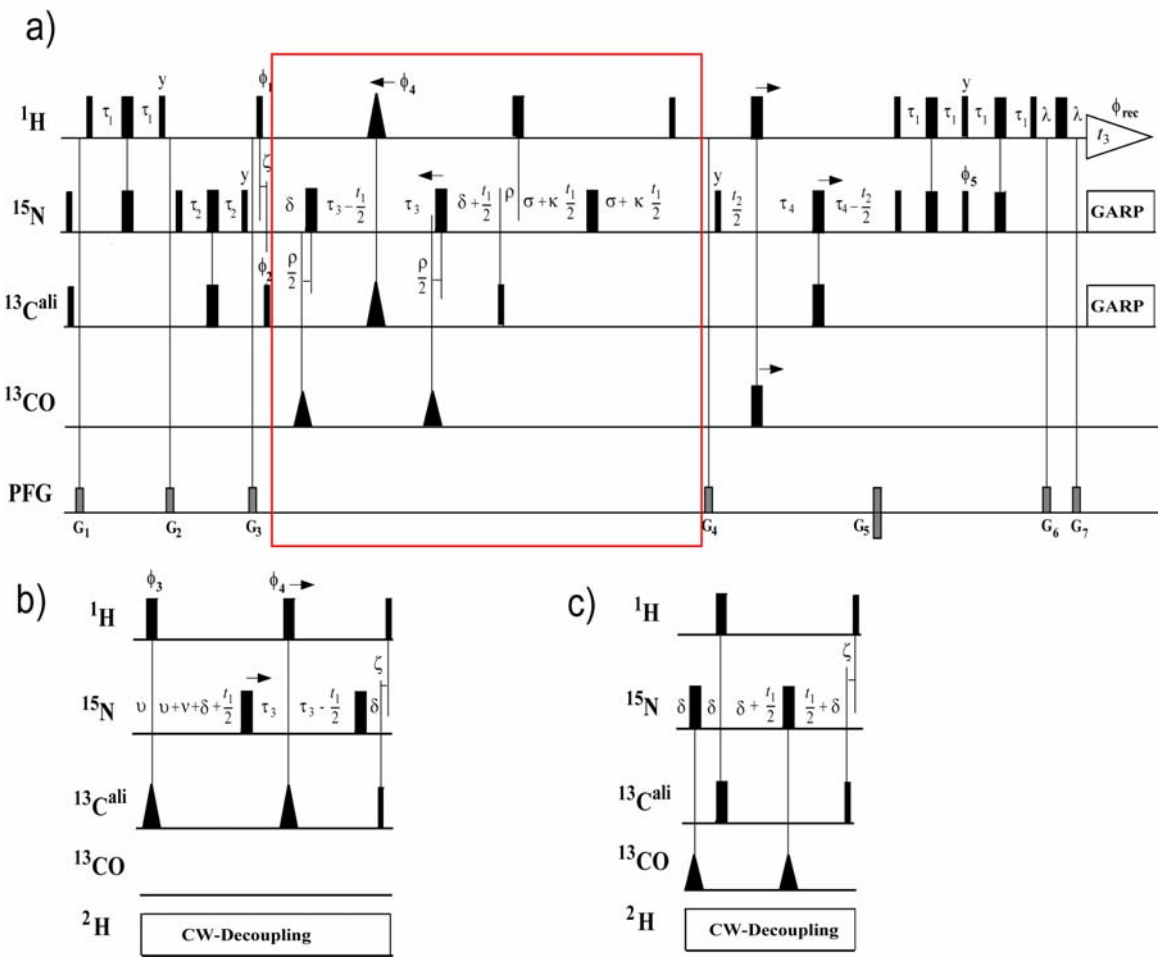

Figure S4. Pulse diagrams of the schemes shown in Figure 1, main text, but including small compensation delays (δ, ν, υ, σ, ρ, ζ) and Bloch-Siegert pulses, used to ensure the absence of frequency-dependent phase errors in the indirectly detected dimensions. The radio-frequency pulses on ^{1}H, ^{15}N, ^{13}C$^\alpha$ and ^{13}C' are applied at 4.7, 120, 56 and 174 ppm, respectively. Narrow and wide bars indicate non-selective 90º and 180º pulses. Triangular pulses on ^{13}C' represent selective 180º-Gaussian pulses of length $p_{C'}^{180}$ = 150 μs, triangular pulses on ^{13}C^{aliphatic} in (a) represent 180º-REBURP pulses of length p_{Cali}^{180} = 400 μs with a full-inversion range of ±33 ppm at 151 MHz ^{13}C frequency, centered at 50 ppm, and in (b) hyperbolic secant pulses of length p_{Cali}^{180} = 700 μs with a full-inversion range of ±80 ppm; the triangular pulse on ^{1}H is a H^N-selective REBURP pulse of length p_H^{180} = 1.5 ms with a full-inversion range of ±2.3 ppm applied at 8.87 ppm. Vertical lines connect centered pulses. ^{15}N- and ^{13}C^{ali}-decoupling is achieved using GARP modulation at RF field strengths, γB_1, of 1.1 kHz and 2.08 kHz, and ^{2}H-decoupling with continuous-wave irradiation using $\gamma B_1 \approx$ 700 Hz (also applied during the N-C$^\alpha$ and C$^\alpha$-N transfers). Unless indicated otherwise, all RF pulses are applied with phase x. Phase cycling: ϕ_3 = {x, x, x, x,-x,-x,-x,-x}; ϕ_4 = {x,-x, x,-x}; ϕ_5 = y; ϕ_{rec} = {x,-x,-x, x}. For spectrum A: ϕ_1 = {x, x,-x,-x}; ϕ_2 = {x,-x, x,-x}. For spectrum B: ϕ_1 = {y, y,-y,-y}; ϕ_2 = {y,-y, y,-y}. A-B (A+B) selects DQ (ZQ) components. The delays have the following values: $\tau_1 = 1/(4J_{H,N})$ = 2.6 ms, $\tau_2 = 1/(4J_{N,C\alpha})$ = 13.7 ms, $\tau_3 = 1/(2J_{C\alpha,C\beta}) - \delta - p_{C'}^{180} - d - 4p_{Cali}^{90}/\pi$ = 13 ms

(where p_{Cali}^{90} is the length of a 90º-pulse on $^{13}C^{\alpha}$ and d is the effective $J_{C\alpha,C\beta}$-coupling time during the $^{13}C^{ali}$- and ^{1}H-180º pulses; in experiment b, $p_{C'}^{180}$ is replaced by p_N^{180}) or 27 ms in b, $\tau_4 = 1/(4J_{N,C\alpha}) = 13.5$ ms , $\delta = 13$ µs, $\upsilon = 4$ µs (required for change of power level on the $^{13}C^{ali}$ channel), $\nu = 4p_{Cali}^{90}/\pi$ for refocusing ^{13}C-chemical-shift evolution and $J_{C\alpha,C'}$ and $J_{C\alpha,H\alpha}$ coupling, $\zeta = 2(p_H^{90}-p_{Cali}^{90})/\pi$ (where p_H^{90} is the length of a 90º-pulse on ^{1}H) for refocusing $^{1}H^{N}$-chemical-shift evolution and $J_{HN,H\alpha}$-coupling, $\lambda = 320$ µs, $\rho = 4p_H^{90}/\pi + 2\sigma + p_N^{180} + \zeta$ is adjusted for exact refocusing of the $^{1}H^{N}$-chemical-shift evolution and $J_{H,N}$-coupling during the total MQ- and SQ-period for $t_1 = 0$, $\sigma = 10$ µs. Pulsed field gradients indicated on the line marked PFG are applied along the z axis (G_{1-4}) or along xyz (G_{5-7}) with duration and strength of: G_1, 500 µs, 18 G/cm; G_2, 300 µs, 36 G/cm; G_3, 500 µs, 18 G/cm; G_4, 250 µs, 15 G/cm; G_5, 3400 µs, -30 G/cm; G_6, 144.75 µs, -30 G/cm; G_7, 200 µs, 30 G/cm. Quadrature detection in the MQ(t_1) and $^{15}N(t_2)$ dimension is achieved by the States-TPPI method applied simultaneously to the phases ϕ_1 and ϕ_2, and by the echo-antiecho method, applied by inversion of G_5 and ϕ_5, respectively. Pulse sequence code for Bruker spectrometers, acquisition parameters, and NMRPipe processing scripts can be downloaded from http://spin.niddk.nih.gov/bax/main.html.

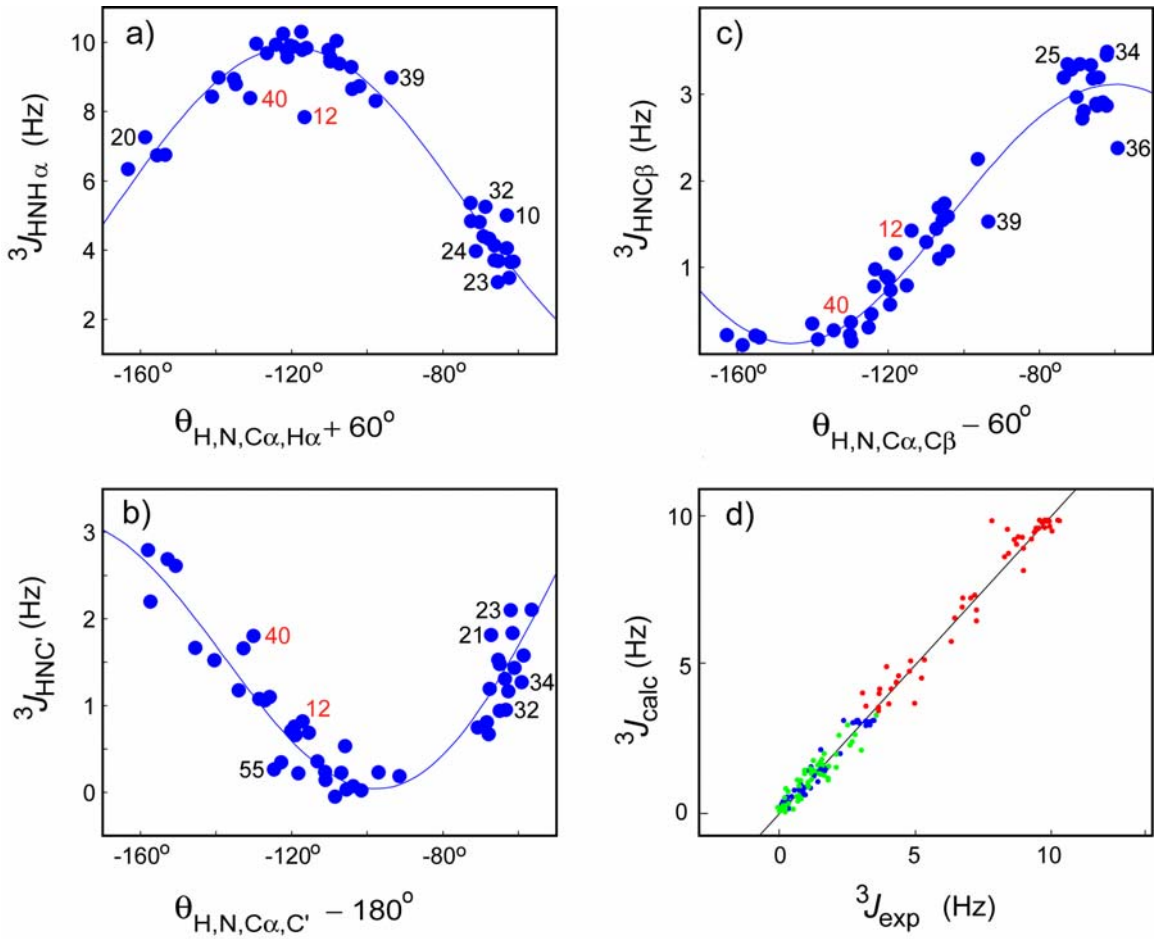

Figure S5. $^3J_{HN,H\alpha}$, $^3J_{HN,C'}$ and $^3J_{HN,C\beta}$ *versus* their respective dihedral angles in the NMR structure, offset by $\pi/3$, π, and $-\pi/3$ for easy comparison of ^3J values, observed for any given residue. Karplus curves shown are derived using singular value decomposition and a static protein structural model (2OED). L12 and D40, previously identified as highly dynamic on the basis of ^{15}N relaxation, are marked in red; residues that deviate more than 1.5 standard deviations from the Karplus curve are marked in black. Marked residues were excluded when fitting the remaining residues to a dynamic Karplus curve with the assumption $\sigma = 10°$. (d) Plot of experimental ^3J values versus values predicted by the static Karplus curve, using dihedral angles taken from the NMR structure, 2OED (red-$^3J_{HN,H\alpha}$; green-$^3J_{HN,C'}$; blue-$^3J_{HN,C\beta}$).

References:

(1) Frisch, M. J.; Trucks, G. W.; Schlegel, H. B.; Scuseria, G. E.; Robb, M. A.; Cheeseman, J. R.; Montgomery, J., J. A.; Vreven, T.; Kudin, K. N.; Burant, J. C.; Millam, J. M.; Iyengar, S. S.; Tomasi, J.; Barone, V.; Mennucci, B.; Cossi, M.; Scalmani, G.; Rega, N.; Petersson, G. A.; Nakatsuji, H.; Hada, M.; Ehara, M.; Toyota, K.; Fukuda, R.; Hasegawa, J.; Ishida, M.; Nakajima, T.; Honda, Y.; Kitao, O.; Nakai, H.; Klene, M.; Li, X.; Knox, J. E.; Hratchian, H. P.; Cross, J. B.; Bakken, V.; Adamo, C.; Jaramillo, J.; Gomperts, R.; Stratmann, R. E.; Yazyev, O.; Austin, A. J.; Cammi, R.; Pomelli, C.; Ochterski, J. W.; Ayala, P. Y.; Morokuma, K.; Voth, G. A.; Salvador, P.; Dannenberg, J. J.; Zakrzewski, V. G.; Dapprich, S.; Daniels, A. D.; Strain, M. C.; Farkas, O.; Malick, D. K.; Rabuck, A. D.; Raghavachari, K.; Foresman, J. B.; Ortiz, J. V.; Cui, Q.; Baboul, A. G.; Clifford, S.; Cioslowski, J.; Stefanov, B. B.; Liu, G.; Liashenko, A.; Piskorz, P.; Komaromi, I.; Martin, R. L.; Fox, D. J.; Keith, T.; Al-Laham, M. A.; Peng, C. Y.; Nanayakkara, A.; Challacombe, M.; Gill, P. M. W.; Johnson, B.; Chen, W.; Wong, M. W.; Gonzalez, C.; Pople, J. A. *Gaussian 03, Revision C.02, Gaussian Inc., Wallingford CT.*, 2004.

(2) Becke, A. D., *J. Chem. Phys.* **1993,** *98*, 5648-5652.

(3) Helgaker, T.; Watson, M.; Handy, N. C., *J. Chem. Phys.* **2000,** *113*, 9402-9409.

(4) Sychrovsky, V.; Grafenstein, J.; Cremer, D., *J. Chem. Phys.* **2000,** *113*, 3530-3547.

(5) Hu, J. S.; Bax, A., *J. Am. Chem. Soc.* **1997,** *119*, 6360-6368.

(6) Bouvignies, G.; Bernado, P.; Meier, S.; Cho, K.; Grzesiek, S.; Bruschweiler, R.; Blackledge, M., *Proc. Natl. Acad. Sci. U. S. A.* **2005,** *102*, 13885-13890.